Supporting Information for Publication

Tunable Dual Visible and Near-Infrared Persistent Luminescence in Doped Zinc Gallogermanate Nanoparticles for Simultaneous Photosensitization and Bioimaging

Liyi Li, Fengjuan Pan, Peter A. Tanner* and Ka-Leung Wong*

Department of Chemistry, Hong Kong Baptist University, Kowloon Tong, Hong Kong S.A.R., China

E-mail addresses: P.A.T.: peter.a.tanner@gmail.com; K.-L. W. klwong@hkbu.edu.hk

Table of Contents	Page

Table S1. Main bands in the FT-IR and Raman spectra in zinc gallogermanates and their assignments from the literature.[S1-S4]

Composition	Type of vibration	FT-IR (cm^{-1})	Raman (cm^{-1})
$ZnGa_2O_4$	[Ga-O-Zn]		609, 714
	[Ga-O] (stretching vibration)	565	
Zn_2GeO_4	[Ge-O-Zn symmetric mode]		745
	[Ge-O-Zn asymmetric mode]		777
	[Ge–O–Ge] (bending vibration)	523	
	tetrahedral [GeO_4] (Ge–O bonds stretching vibration)	733	802
GeO_2	tetrahedral [GeO_4] (Ge–O stretching vibration)	865	885
	tetrahedral [GeO_4] (Ge–Ge stretching vibration)		521

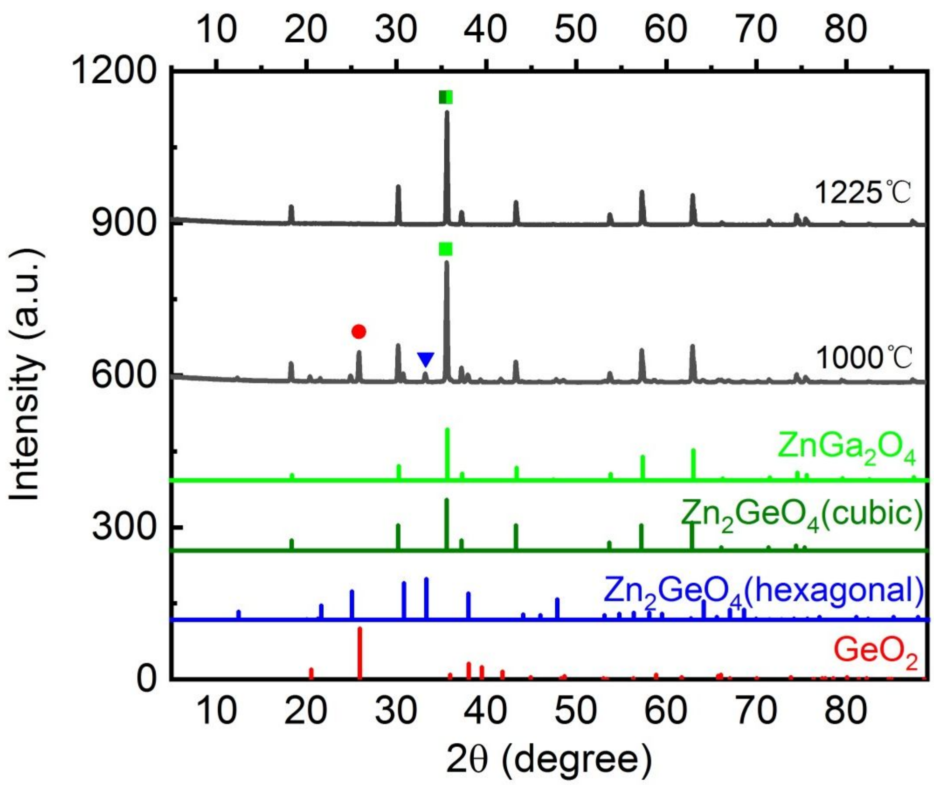

Figure S1. XRD powder diffraction patterns of zinc gallogermanate (1-1-1) synthesized at 1000 ^{o}C and 1225 ^{o}C. The green, dark green, blue and red lines represent $ZnGa_2O_4$ (PDF# 38-1240), cubic Zn_2GeO_4 (PDF#25-1018) hexagonal Zn_2GeO_4 (PDF#11-0687) and GeO_2 (PDF#43-1016), respectively.

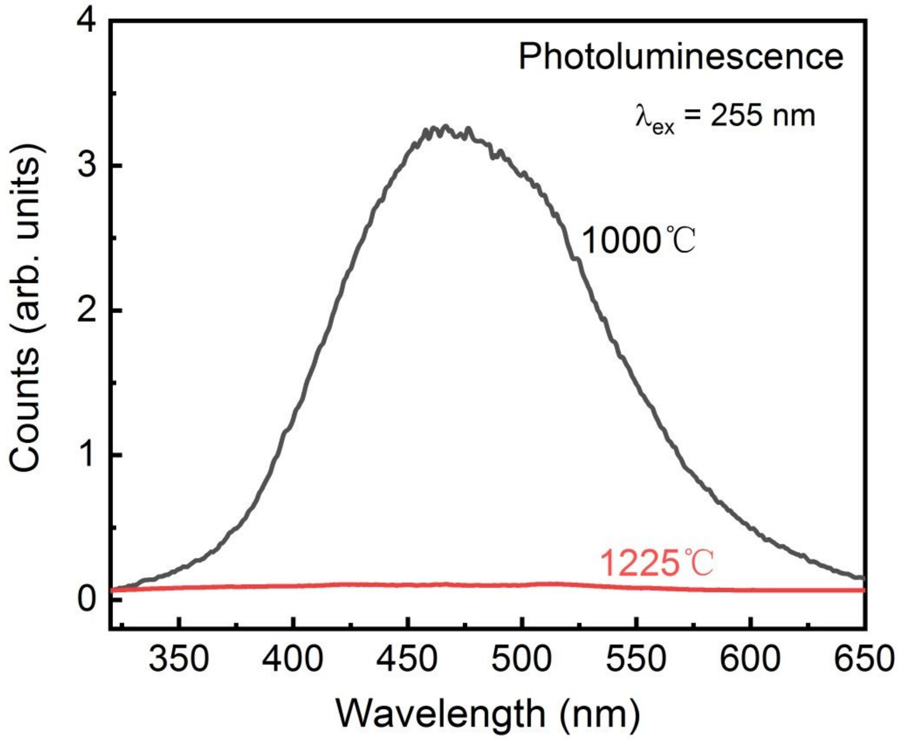

Figure S2. Photoluminescence spectra of samples 1-1-1 prepared at 1000 and 1225 ^{o}C using 255 nm excitation.

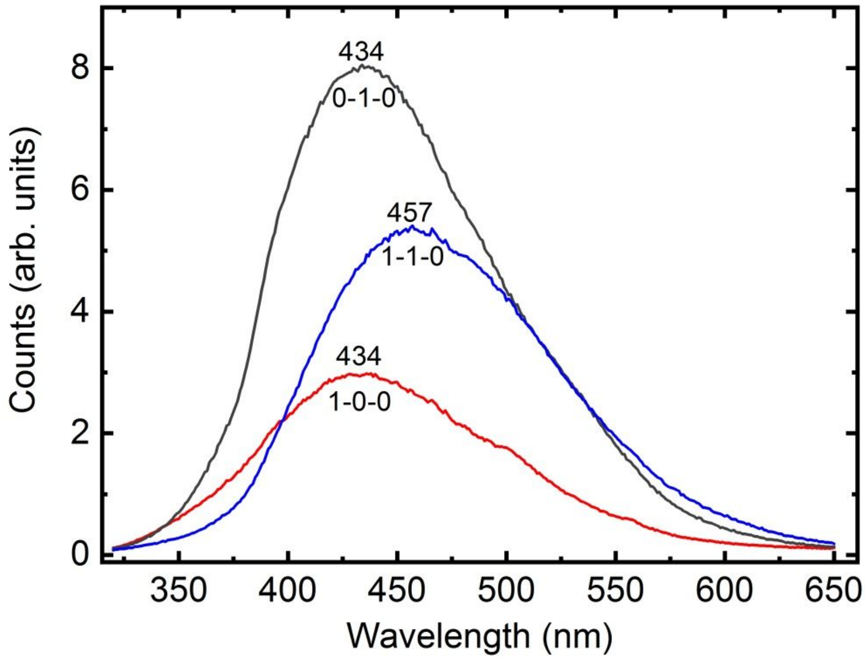

Figure S3. Emission spectra of 1-0-0, 0-1-0 and 1-1-0 samples under 255 nm excitation.

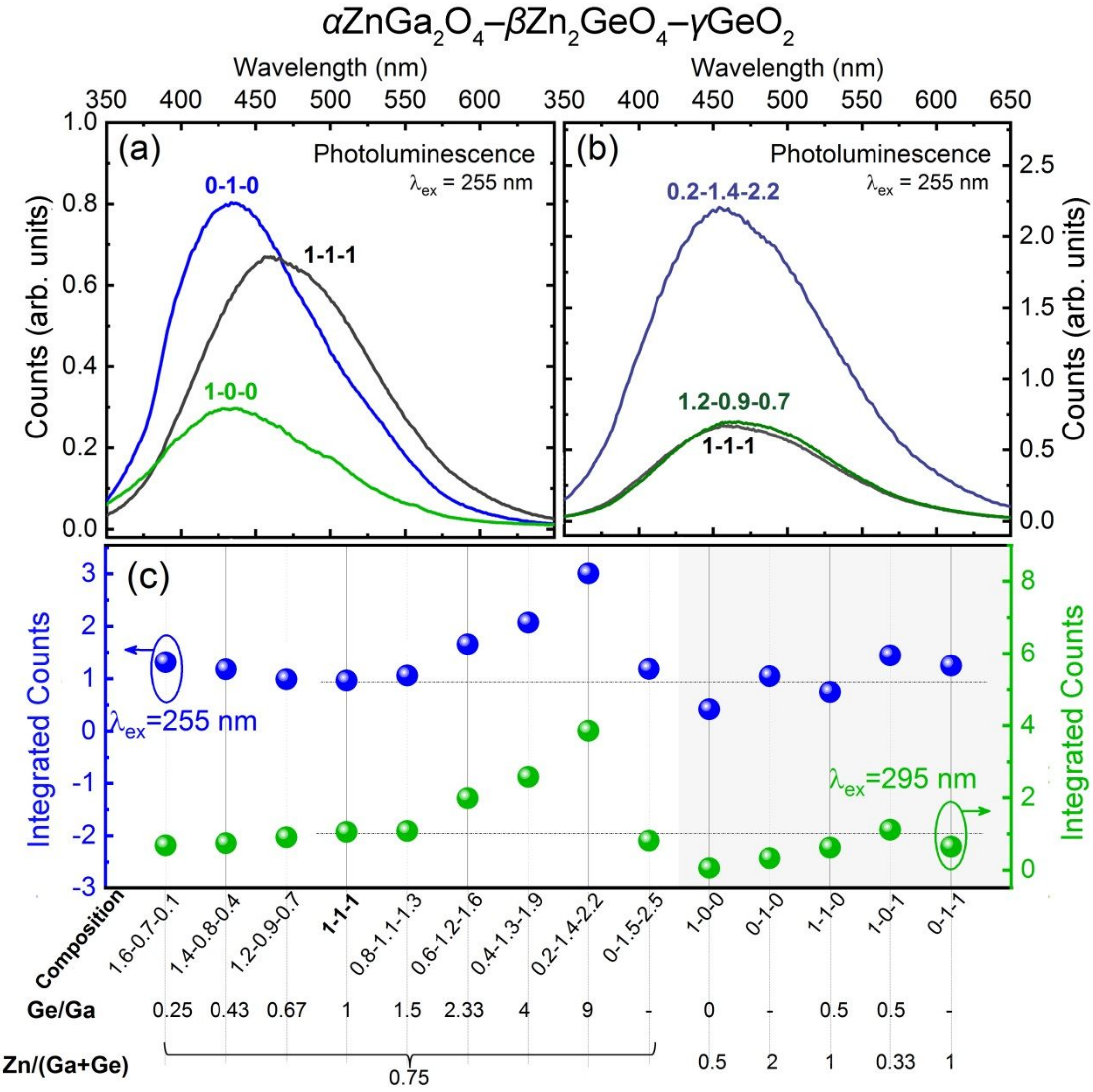

Figure S4. (a) Emission spectra of sample 1-0-0, 0-1-0 and 1-1-1 under the 255 nm excitation; (b) Emission spectra of sample 0.2-1.4-2.2, 1-1-1 and 1.2-0.9-0.7 under 255 nm excitation; (c) Comparison of integrated emission intensity of various samples under 255 and 295 excitation.

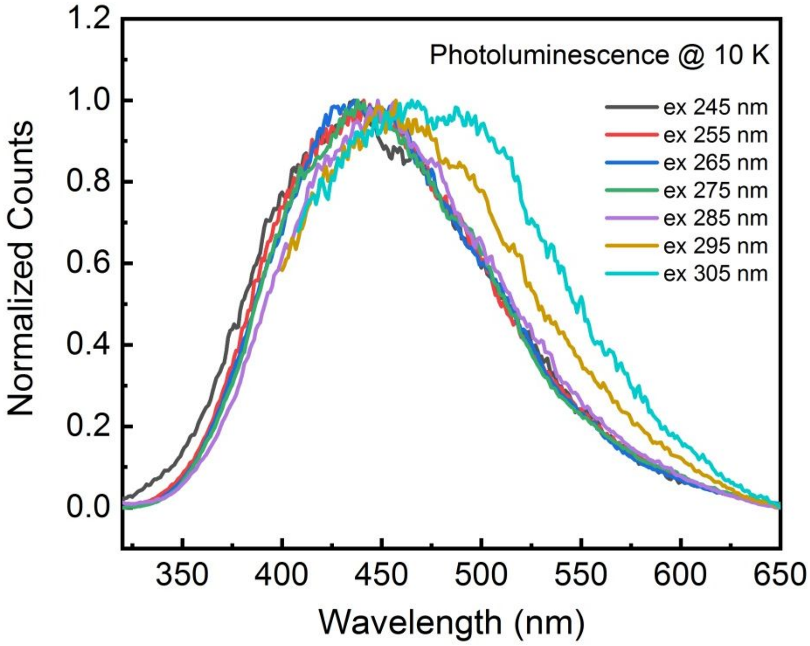

Figure S5. Circa 10 K emission spectra of 1-1-1 under different excitation wavelengths.

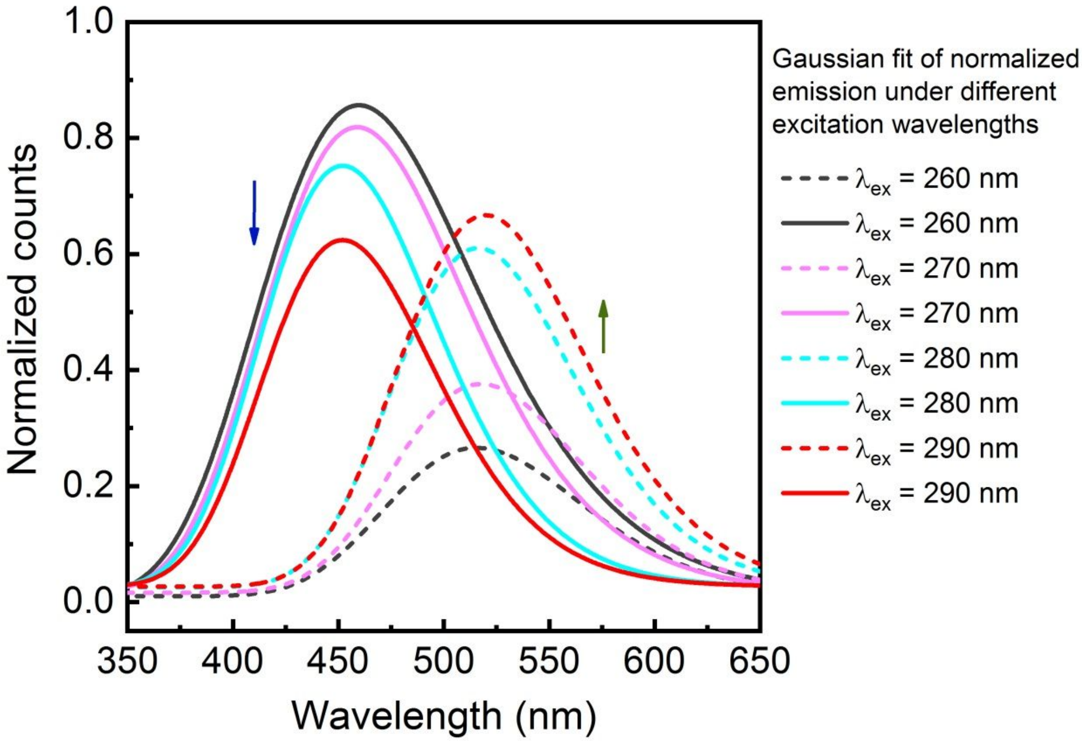

Figure S6. Deconvoluted emission of 1-1-1 into two Gaussians under various excitation wavelengths.

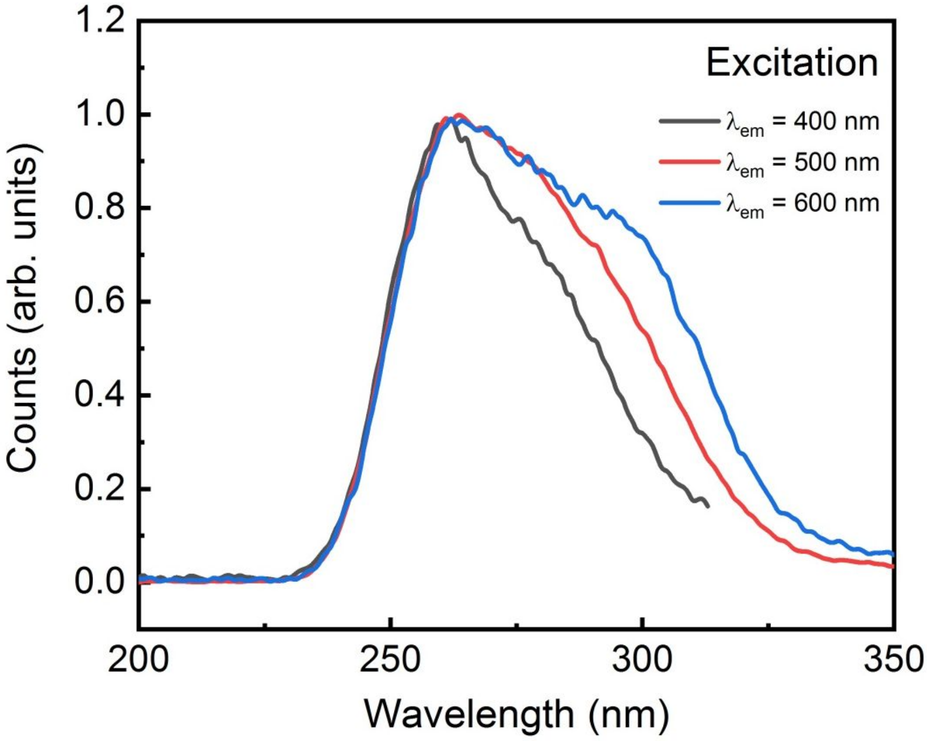

Figure S7. Excitation spectra of 1-1-1 when monitoring different emission wavelengths.

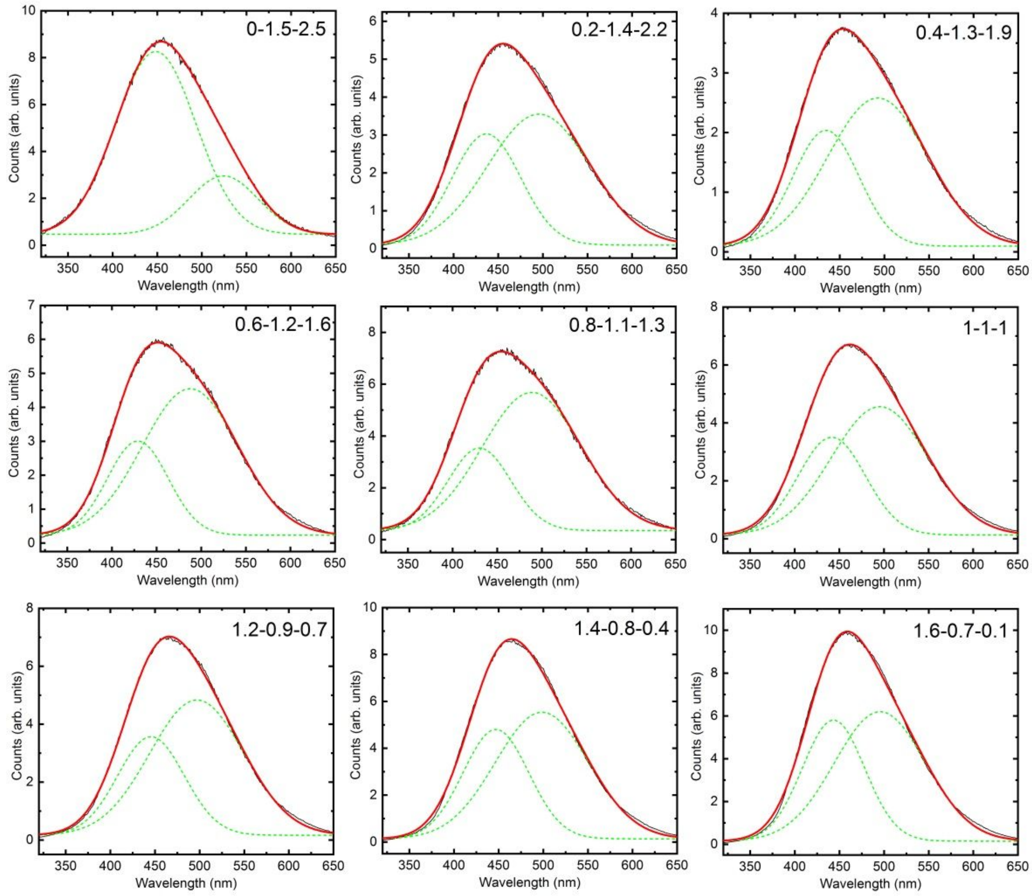

Figure S8. 255 nm excited emission spectra of zinc gallogermanates $\alpha ZnGa_2O_4$–βZn_2GeO_4–γGeO_2, α, β, $\gamma \neq 0$. Each spectrum is fitted by two Gaussian bands (green) with the sum indicated by a red line.

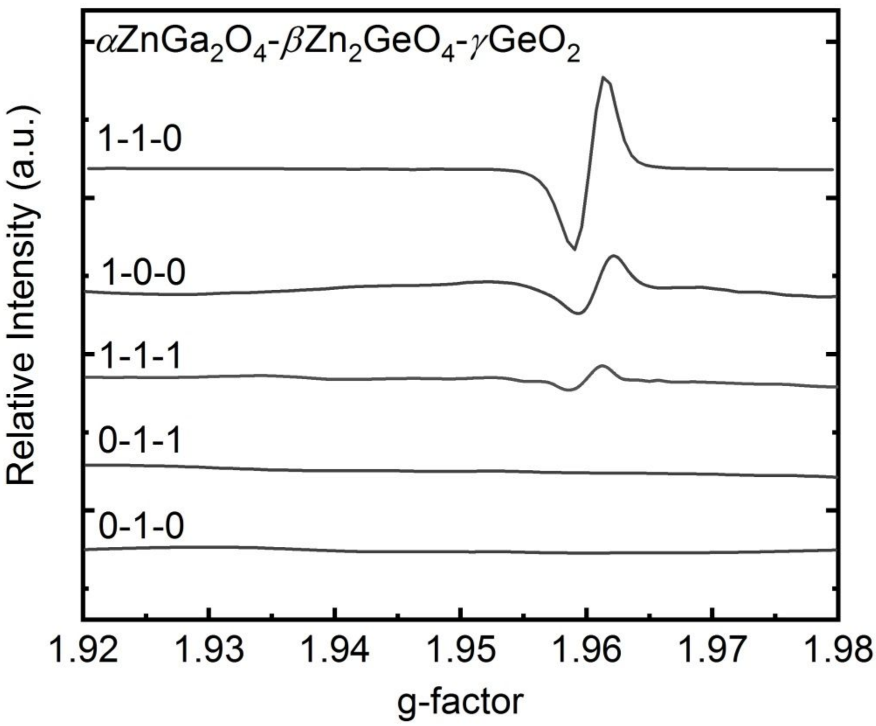

Figure S9. ESR spectra at 100 K of samples 1-1-0,1-0-0, 1-1-1, 0-1-1, 0-1-0.

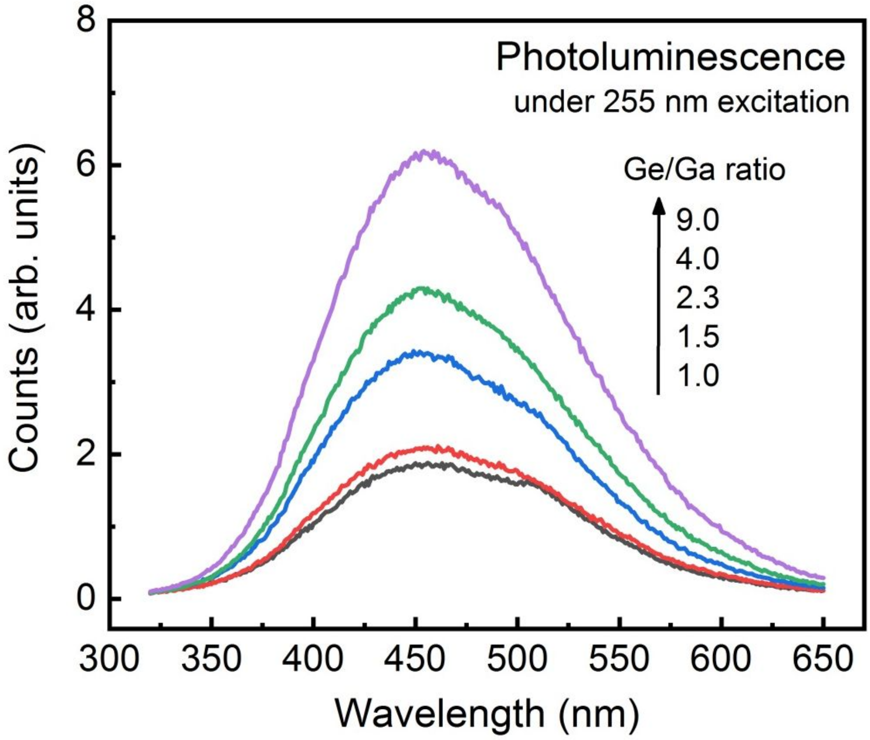

Figure S10. Dependence of PL spectra on different Ge/Ga ratio.

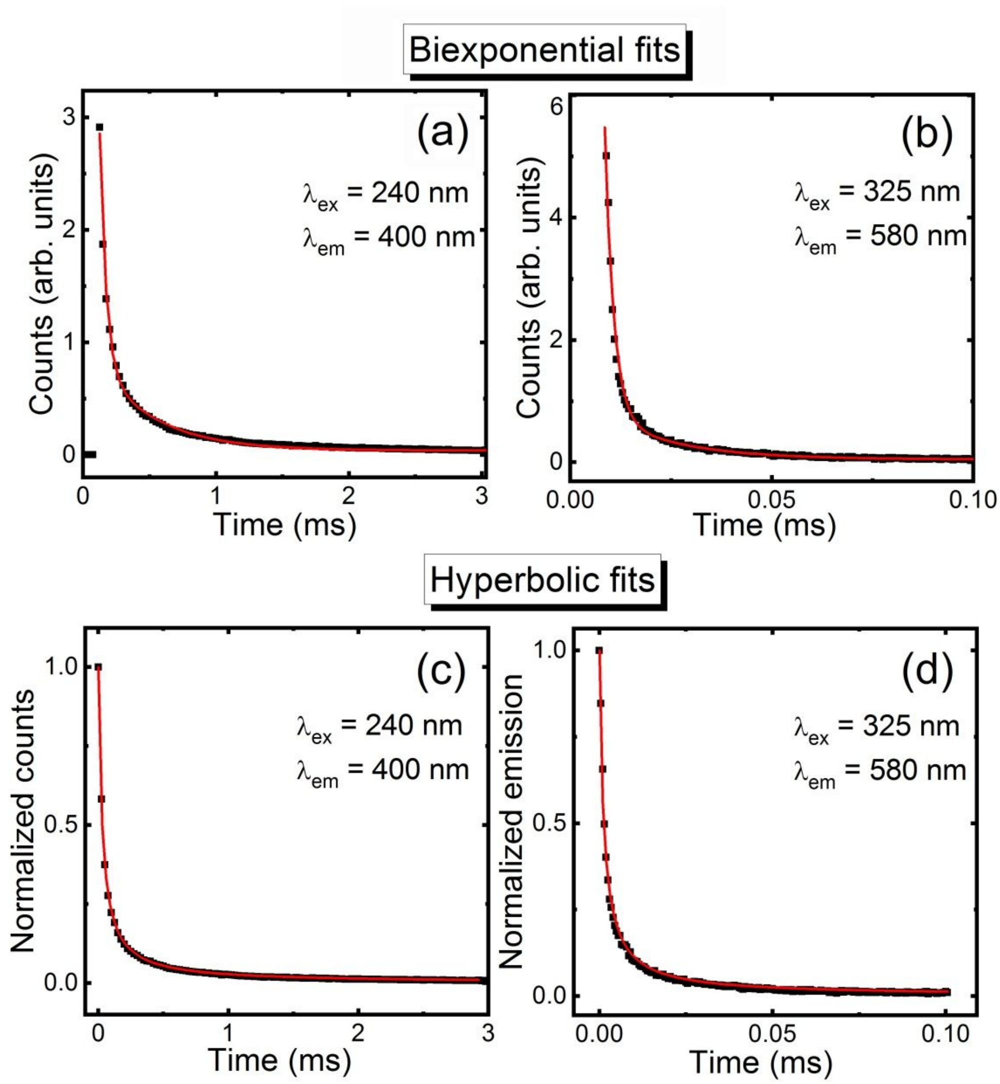

Figure S11. Examples of biexponential decay curve fits using excitation with a ~2 microsecond pulsed laser: (a) excitation at 240 nm and emission at 400 nm;

Fitting y = 387±16 + (9838±322)×exp(-x/(0.44±0.01)) + (286284±15847)×exp(-x/0.048±0.001), R^2_{adj} = 0.98762, with time in ms; (b) excitation at 325 nm and emission at 580 nm: Fitting y = 44±13 + (1092±172)×exp(-x/(18.9±2.6)) + (209146±26684)×exp(-x/2.24±0.08), R^2_{adj} = 0.98762, with time in μs. Examples of hyperbolic fits: (c) excitation at 240 nm and emission at 400 nm; Fitting y = 1/(1+(34.09±0.27)x), R^2_{adj} = 0.99821, with B in (ms)$^{-1}$; (d) excitation at 325 nm and emission at 580 nm: Fitting y = 1/(1+(778±12)x), R^2_{adj} = 0.99821, with B in (ms)$^{-1}$.

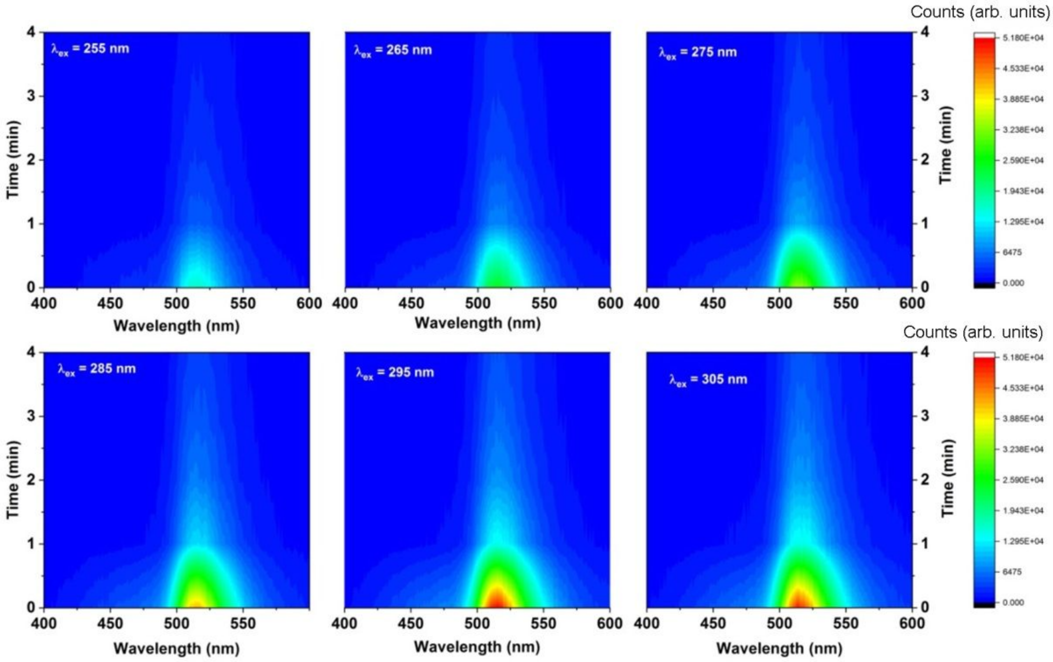

Figure S12. Persistent luminescence spectra of sample 1-1-1 using different excitation wavelengths.

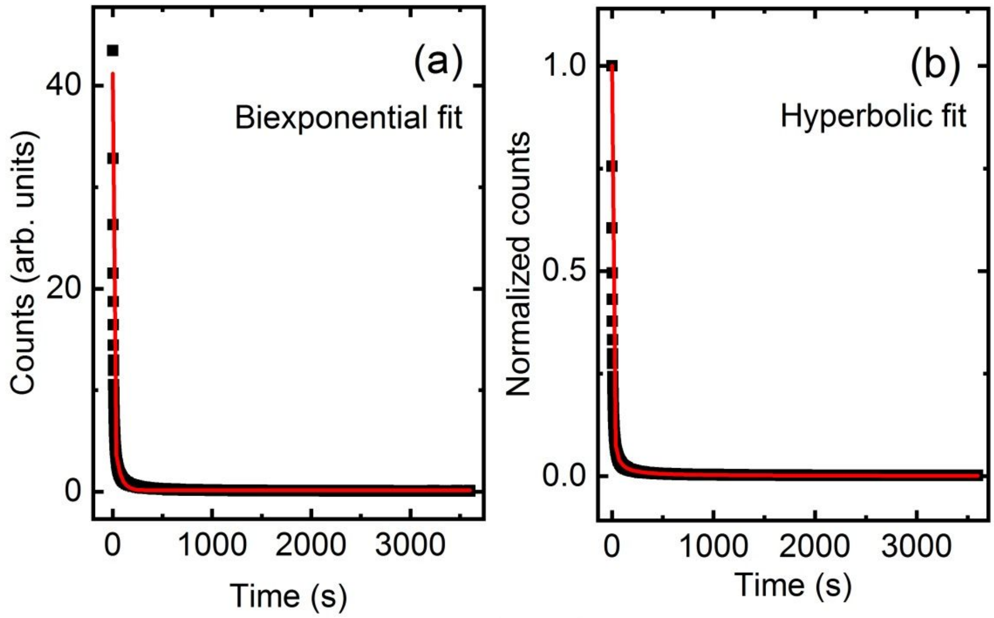

Figure S13. (a) Biexponential data fit 0-3600 s to persistent luminescence decay in Figure 7: sample 1-1-1 after 10 min excitation at 295 nm.

Fits to persistent luminescence decay in Figure 7:

Time: 0-3600 s

y =(1310±22) + (340877±1111)×exp[-x/(4.15±0.03)] + (69442±662)×exp[-x/(51.9±0.5)], R^2_{adj} = 0.9906

Fraction of emission with shorter lifetime = $A_1\tau_1/(A_1\tau_1 + A_2\tau_2)$ = 0.72

Time 101-3600 s

y = (733±4) + (20057±204)×exp[-x/(96±1)] + (4017±58)×exp[-x/(586±7)], R^2_{adj} = 0.9927

Fraction of emission with shorter lifetime = 0.45

Time 201-3600 s

y = (700±5) + (13099±355)×exp[-x/(135±3)] + (3059±78)×exp[-x/(709±15)], R^2_{adj} = 0.9848

Fraction of emission with shorter lifetime = 0.45

Time 301-3600 s

y = (681±7) + (8879±450)×exp[-x/(177±8)] + (2520±116)×exp[-x/(805±28)], R^2_{adj} = 0.9741

Fraction of emission with shorter lifetime = 0.44

(b) Hyperbolic data fit 0-3600 s to persistent luminescence decay in Figure 7: sample 1-1-1 after 10 min excitation at 295 nm.

Fits to persistent luminescence decay in Figure 7:

Time: 0-3600 s

y = 1/(1+(0.3397±0.0003)x), R^2_{adj} = 0.99931.

Time 101-3600 s

y = 1/(1+(0.00836±0.00003)x), R^2_{adj} = 0.97137.

Time 201-3600 s

y = 1/(1+(0.00347±0.00001)x), R^2_{adj} = 0.95399.

Time 301-3600 s

y = 1/(1+(0.00245±0.00001)x), R^2_{adj} = 0.91911.

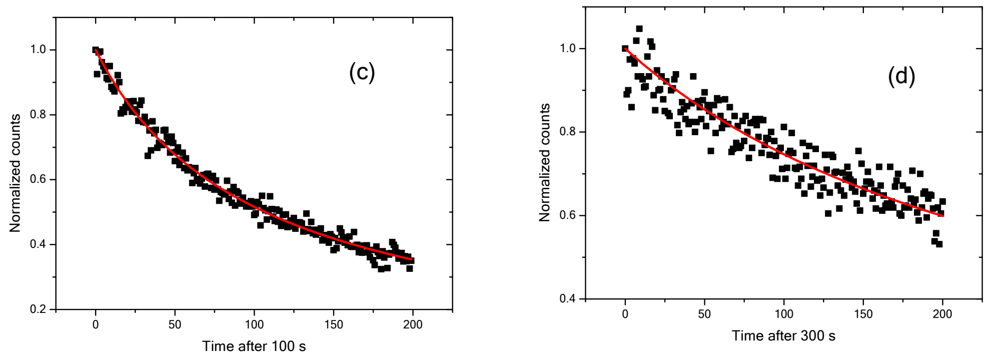

Figure S13. Persistent luminescence decay curve of sample 1-1-1 after 5 min excitation at 295 nm: (c) from 100 s to 300 s; (d) from 300 s to 500 s. Fitting with the one-parameter DHARA function, Eq. (4), without refining the value of c (taken as c = 1.1) gives the values of k of 0.00972 s^{-1} (in c) and 0.00344 s^{-1} (in d). These correspond to lifetimes τ(100-300) = 103 s and τ(300-500) = 291 s.

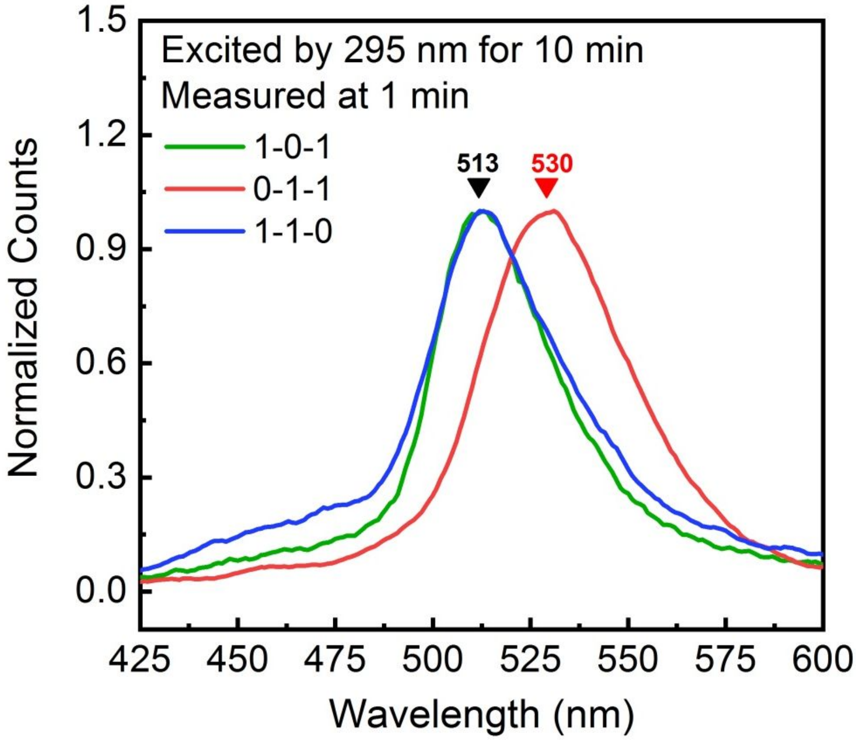

Figure S14. Persistent luminescence spectra of 1-0-1, 0-1-1 and 1-1-0 measured at 1 min after 10 min excitation at 295 nm.

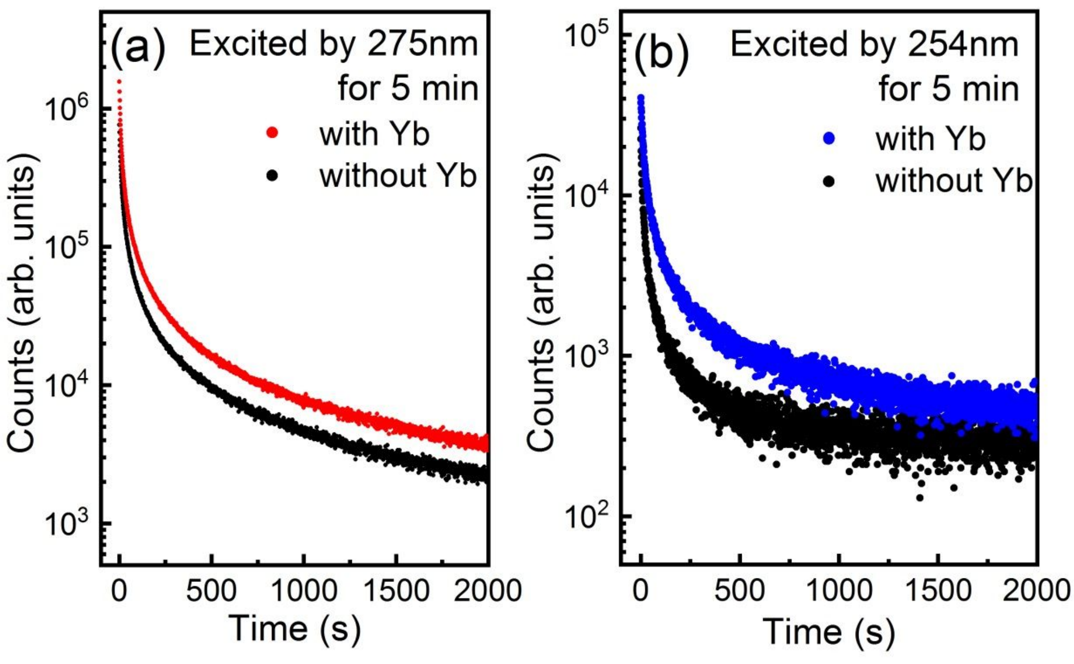

Figure S15. Co-doped 1-1-1 sample with Cr^{3+} (0.5 mol%) with or without 1.5 mol% Yb^{3+}: (a) NIR (698 nm) persistent luminescence decay curves; (b) blue (465 nm) persistent luminescence decay curves.

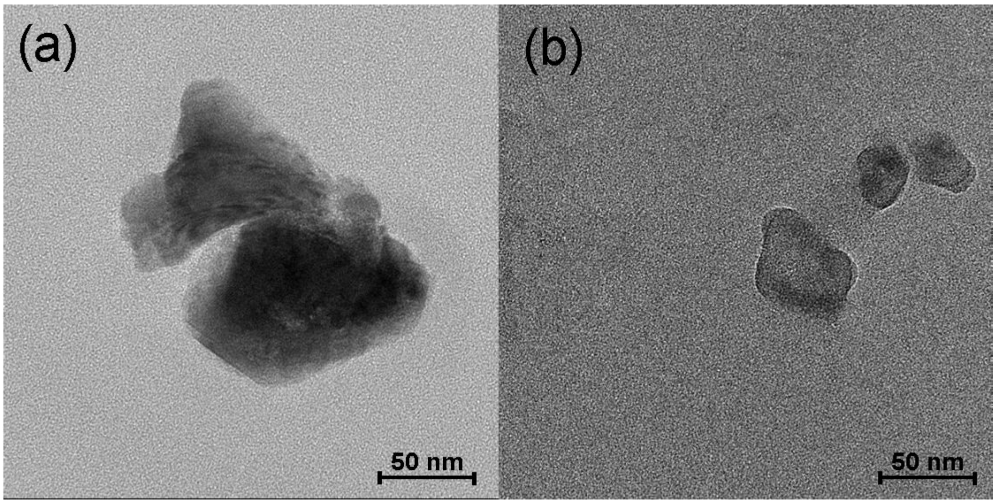

Figure S16. Synthesized nanoparticles to demonstrate the change in size without (a) and with (b) Yb^{3+} co-doping. The approximate sizes are 80 nm in (a) and 30 nm in (b).

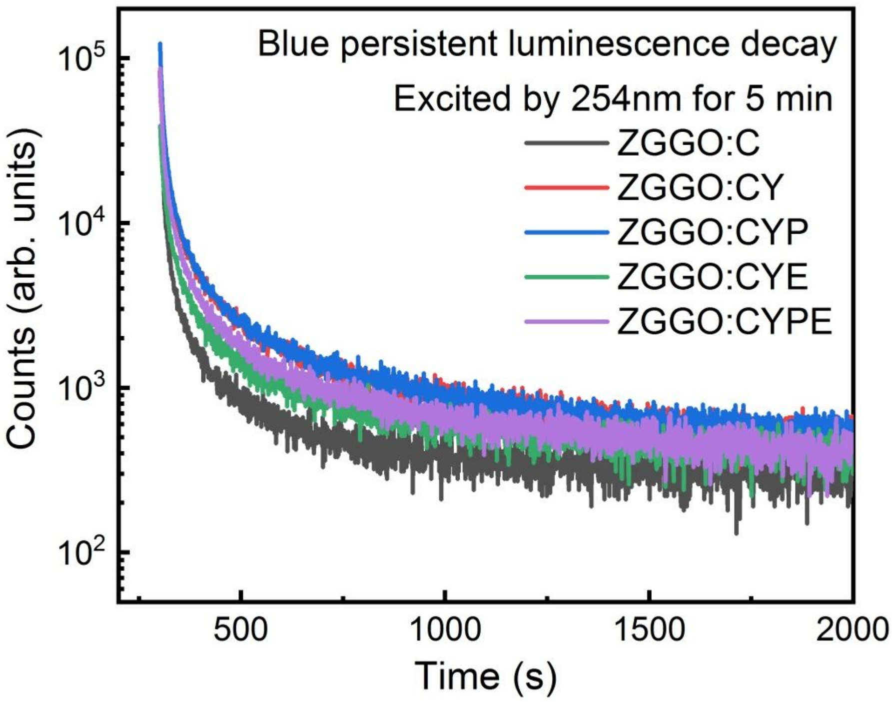

Figure S17. (a) Blue persistent luminescence decay curves of co-doped $Zn_3Ga_2Ge_2O_{10}$:Cr^{3+} (ZGGO: C) samples: $Zn_3Ga_2Ge_2O_{10}$:Cr^{3+}, Yb^{3+} (ZGGO: CY), $Zn_3Ga_2Ge_2O_{10}$:Cr^{3+}, Yb^{3+}, Pr^{3+} (ZGGO: CYP), $Zn_3Ga_2Ge_2O_{10}$:Cr^{3+}, Yb^{3+}, Er^{3+} (ZGGO: CYE), and $Zn_3Ga_2Ge_2O_{10}$:Cr^{3+}, Yb^{3+}, Pr^{3+}, Er^{3+} (ZGGO: CYPE) under 254 nm excitation for 5 min.

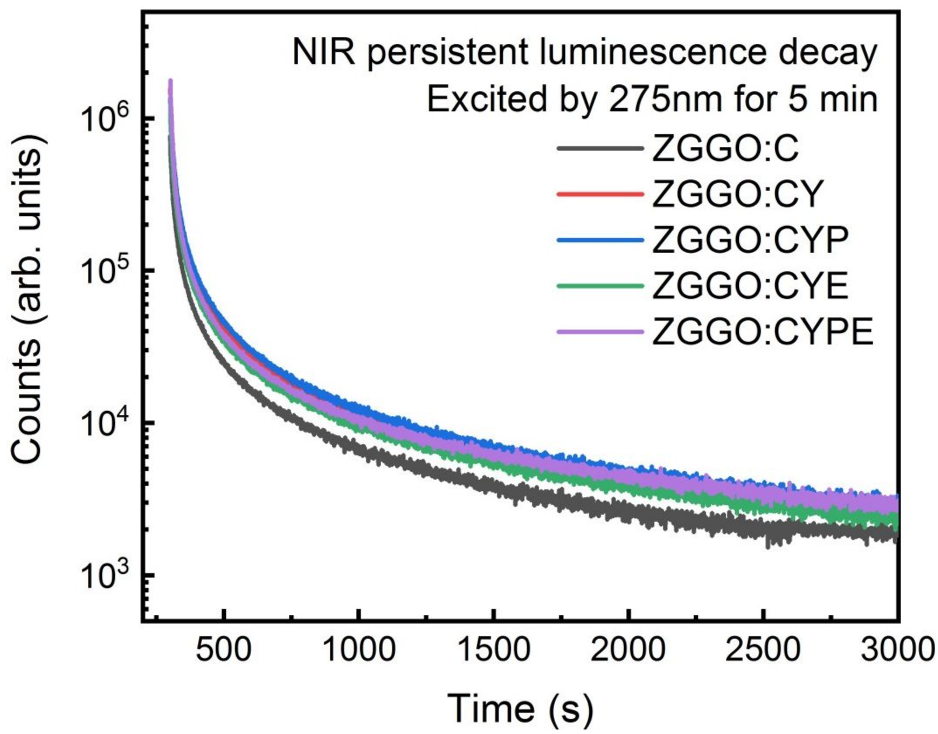

Figure S18. NIR persistent luminescence decay curves of co-doped ZGGO samples: $Zn_3Ga_2Ge_2O_{10}$:Cr^{3+} (ZGGO: C), $Zn_3Ga_2Ge_2O_{10}$:Cr^{3+}, Yb^{3+} (ZGGO: CY), $Zn_3Ga_2Ge_2O_{10}$:Cr^{3+}, Yb^{3+}, Pr^{3+} (ZGGO: CYP), $Zn_3Ga_2Ge_2O_{10}$:Cr^{3+}, Yb^{3+}, Er^{3+} (ZGGO: CYE), and $Zn_3Ga_2Ge_2O_{10}$:Cr^{3+}, Yb^{3+}, Pr^{3+}, Er^{3+} (ZGGO: CYPE) under 274 nm excitation for 5 min.

Table S2. Relationship between phase ratio and Ga/Ge ratio.

Phase ratio $\alpha ZnGa_2O_4$–βZn_2GeO_4–γGeO_2	Ga/Ge ratio	Phase ratio $\alpha ZnGa_2O_4$–βZn_2GeO_4–γGeO_2	Ga/Ge ratio
1-1-1	1.0	0.2-1.4-2.2	0.11
0-1-1	0.0	0.6-1.2-1.6	0.43
1-0-1	2.0	0.4-1.3-1.9	0.25
1-1-0	2.0	0-1.5-2.5	0.0
0-1-0	0.0	1.4-0.8-0.4	2.33
1-0-0	∞	1.6-0.7-0.1	4.0
1.2-0.9-0.7	1.5	0.8-1.1-1.3	0.67

Table S3. Summary of defect sites found or inferred to be present in ZGGO :Cr^{3+}

Type of defect site	**Evidence**
$Ga^{\bullet}_{Zn}$ and Zn'_{Ga} antisite defects	These are well-documented for the spinel structure.[S6-S8]
Oxygen vacancy ($V^{\bullet}_{O}$) and interstitial zinc ($Zn^{\bullet}_{i}$) with germanium vacancy (V_{Ge}) or zinc vacancy (V'_{Zn}) acceptors.	Well documented in spinels.[S9-S12]
Donor (e.g. $V^{\bullet}_{O}$) – acceptor (e.g. $(V_O - V_{Ga})'$) recombination.	Luminescence is enhanced with the replacement of Ga^{3+} by Ge^{4+}.
Oxygen vacancy ($V^{\bullet}_{O}$).	Synthesis of ZGGO 1-1-1 in ambient and reduced atmospheres
$Ge^{\bullet}_{Ga}$. The $Ga^{\bullet}_{Zn}$ and Zn'_{Ga} antisite defects.	Zn deficiencies have a greater impact upon the increase in luminescence intensity.
Singly charged oxygen vacancy $V^{\bullet}_{O}$, (type F^{+} center)	ESR g-factor at 1.9599.
Zinc vacancy V'_{Zn}.	ESR g-factor at 2.0109.
Singly charged oxygen vacancy $V^{\bullet}_{O}$.	Increasing the Ga/Ge ratio increases ESR intensity of band with g-factor at 1.9599.
Other non-paramagnetic defect centers such as F center.	ESR intensity of the $V^{\bullet}_{O}$ band in different samples does not follow the same pattern as the photoluminescence intensity.
Other types of defect center (for example, F_A and F).	The reported decay lifetimes of oxygen vacancy defects are in the ns range.[S10] However, ms lifetimes have been reported for defects such as the F_A center in CaO:Mg,[S13] and the F centers in Al_2O_3, YAP and YAG.[S14] Our measured emission decay is much longer at shorter wavelengths (Figures S11a and b).

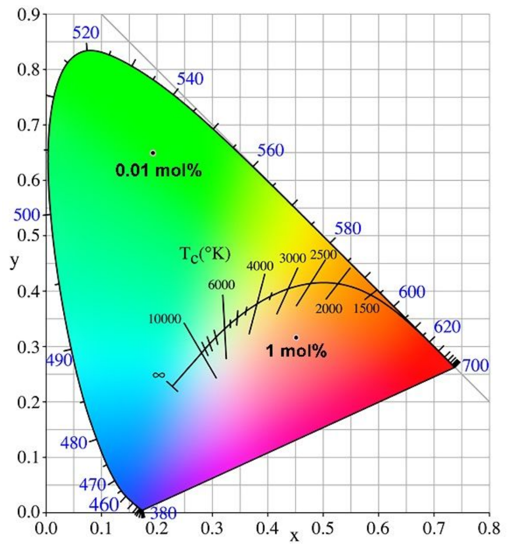

Figure S19. CIE diagram for samples of 1-1-1 doped with 0.01 mol% and 1.0 mol% Cr^{3+}. The two points are marked on the diagram.

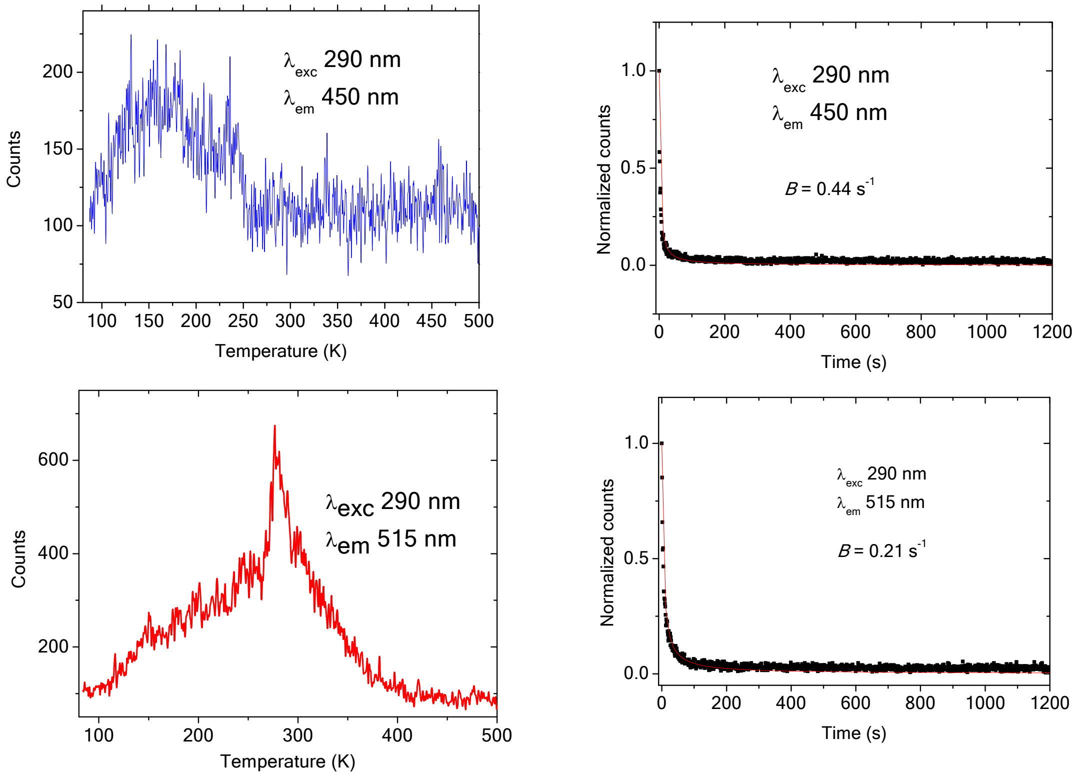

Figure S20. Thermoluminescence curves for undoped sample 1-1-1.

Excitation wavelength: 290nm; Emission wavelengths: 450 nm and 515 nm. Experiment procedure: Excitation for 10 min at 85 K.

Right hand side: persistent luminescence decay at 85 K for 20 min: the fitted values of *B* from hyperbolic fits are indicated;

Left hand side: the following thermoluminescence curve from 85 – 507 K.

References

S1. Ren, J.; Xu, X.; Zeng, H.; Chen, G.; Kong, D.; Gu, C.; Chen, C.; Liu, Z.; Kong, L.; Setlur, A. Novel Self-Activated Zinc Gallogermanate Phosphor: The Origin of Its Photoluminescence. *J. Am. Ceram. Soc.* **2014**, *97*, 3197-3201.

S2. Ardyanian, M.; Rinnert, H.; Devaux, X.; Vergnat, M. Structure and Photoluminescence Properties of Evaporated GeO_x Thin Films. *Appl. Phys. Lett.* **2006**, *89*, 011902.

S3. Pascuta, P.; Culea, E. FTIR Spectroscopic Study of Some Bismuth Germanate Glasses Containing Gadolinium Ions. *Mater. Lett.* **2008**, *62*, 4127-4129.

S4. Madon, M.; Gillet, Ph.; Julien, Ch.; Price, G. D. A Vibrational Study of Phase Transitions Among the GeO_2 Polymorphs. *Phys. Chem. Minerals* **1991**, *18*, 7-18.

S5. Whitehead, L.; Whitehead, R.; Valeur, B.; Berberan-Santos, M. A Simple Function for the Description of Near-Exponential Decays: the Stretched or Compressed Hyperbola. *Am. J. Phys.* **2009**, *77*, 173-179.

S6. Allix, M.; Chenu, S.; Véron, E.; Poumeyrol, T.; Kouadri-Boudjelthia, E. A.; Alahraché, S.; Porcher, F.; Massiot, D.; Fayon, F. Considerable Improvement of Long-Persistent Luminescence in Germanium and Tin Substituted $ZnGa_2O_4$. *Chem. Mater.* **2013**, *25*, 1600-1606.

S7. Bessière, A.; Sharma, S. K.; Basavaraju, N.; Priolkar, K. R.; Binet, L.; Viana, B.; Bos, A. J. J.; Maldiney, T.; Richard, C.; Scherman, D.; Gourier, D. Storage of Visible Light for Long-Lasting Phosphorescence in Chromium-Doped Zinc Gallate. *Chem. Mater.* **2014**, *26*, 1365-1373.

S8. De Vos, A.; Lejaeghere, K.; Vanpoucke, D. E. P. ; Joos, J. J.; Smet, P. F.; Hemelsoet, K. First-Principles Study of Antisite Defect Configurations in $ZnGa_2O_4$:Cr Persistent Phosphors. *Inorg. Chem.* **2016**, *55*, 2402-2412.

S9. Xie, Z.-Y.; Lu, H.-L.; Zhang, Y.; Sun, Q.-Q.; Zhou, P.; Ding, S.-J.; Zhang, D. W. The Electronic Structures and Optical Properties of Zn_2GeO_4 with Native Defects. *J. Alloys Compds.* **2015**, *619*, 368-371.

S10. Liu, Z.; Jing, X.; Wang, L. Luminescence of Native Defects in Zn_2GeO_4. *J. Electrochem. Soc.* **2007**, *154*, H500-H506.

S11. Wan, M.; Wang, Y.; Wang, X.; Zhao, H.; Li, H.; Wang, C. Long Afterglow Properties of Eu^{2+}/Mn^{2+} Doped Zn_2GeO_4. *J. Lumin.* **2014**, *145*, 914-918.

S12. Ren, J.; Xu, X.; Zeng, H.; Chen, G.; Kong, D.; Gu, C.; Chen, C.; Liu, Z.; Kong, L.; Setlur, A. Novel Self-Activated Zinc Gallogermanate Phosphor: The Origin of its Photoluminescence. *J. Am. Ceram. Soc.* **2014**, *97*, 3197-3201.

S13. Welch, L. S.; Hughes, A. E. Luminescence of the F_A Centre in CaO: Mg. *J. Phys. C: Solid State Phys*. **1980**, *13*, 5801-10.

S14. Zorenko, Y.; Zorenko, T.; Voznyak, T.; Mandowski, A.; Xia, Q.; Batentschuk, M.; Friedrich, J. Luminescence of F^+ and F Centers in Al_2O_3-Y_2O_3 Oxide Compounds. *IOP Conf. Ser.: Mater. Sci. Eng.* **2010**, *15*, 012060.